Orbital antiferromagnetism in coupled planar systems

D. F. Schroeter*
Department of Physics, Reed College, Portland, Oregon 97202, USA

S. Doniach
Department of Physics, Stanford University, Stanford, California 94305, USA

(Received 5 August 2003; revised manuscript received 23 October 2003; published 12 March 2004)

A realistic model for the electronic structure of $SrRuO_3$ is examined to determine the possibility of orbital antiferromagnetic order in this material. By calculating the susceptibility to orbital and spin antiferromagnetic order, it is shown that the band structure of $SrRuO_3$ serves to destabilize the Néel ordered state and that the susceptibility to orbital antiferromagnetic order is larger over a range of doping. The resultant orbital antiferromagnetic state consists of coupled two-dimensional planes. The effect of the coupling on the planar system is calculated; the energy shifts of different configurations depend only on the total current in the sample and are linear in this quantity. An orbital antiferromagnetic ground state is found which has no net current flowing along the bonds.

DOI: 10.1103/PhysRevB.69.094407 PACS number(s): 75.10.Lp, 71.10.Fd, 71.30.+h

It has recently been proposed[1,2] that the pseudogap observed[3] in the transition-metal oxide $SrRuO_3$ above its ferromagnetic transition temperature of $T_C \approx 150$ K may be explained by a three-dimensional version of the flux states invented by Affleck and Marston.[4] As suggested by Ahn,[5] $SrRuO_3$ appears to be near a Mott transition as can be seen from doping with calcium to form $Ca_xSr_{1-x}RuO_3$. The on-site Coulomb repulsion is most likely in the range of $U = 3$–5 eV, as estimated from photoemission[6] and optical conductivity measurements.[5] The resistivity has been observed to pass through the Ioffe-Regel limit without saturation,[7] a behavior indicative of a ''bad metal.''[8] In addition to the peak at low frequencies ($\omega \approx 250$ cm^{-1}) which leads us to identify the state as pseudogapped, at high frequency the optical conductivity scales with the non-Fermi liquid value of $\omega^{-1/2}$.[3]

In this paper, the nature of the orbital antiferromagnetic (OAF), or flux-phase, order in $SrRuO_3$ is revisited using a multiband model which encompasses the key features of the material's electronic structure. Precisely how the electronic structure affects the susceptibility to form an OAF state is calculated and compared to the case of a spin antiferromagnet (SAF) or Néel state. While $SrRuO_3$ is a three-dimensional material, its band structure consists of sets of intersecting planar sheets. We show how the orbital antiferromagnetic order develops in these planes and how coupling between intersecting planes determines the configuration of currents in the material. Models proposing different mechanisms for the non-Fermi-liquid behavior of $SrRuO_3$ have been proposed by Laad and Müller-Hartmann[9] and Liebsch.[10] While the pseudogap in $SrRuO_3$ only appears above T_C, we propose that this is due to the ferromagnetic state being preferred below this point. As such, we are considering in this paper only the state at zero temperature and investigating the effects of a realistic electronic band structure on the stability of the orbital antiferromagnetic ground state.

I. BAND STRUCTURE

$SrRuO_3$ has an orthorhombic crystal structure, becoming strictly cubic at temperatures greater than 900 K.[11] There are five bands crossing the Fermi surface formed by hybridizing the ruthenium d orbitals and oxygen p orbitals. As a starting point for our model we use the Slater-Koster parameters obtained by Mazin[12] using the linear augmented plane-wave method with a set of 14 bands at 165 momentum points in the Brillouin zone. We restrict our attention to the three bands formed from the hybridized t_{2g}-p_π orbitals. As pointed out by Mazin, the band structure contains nearly-flat bands between Γ and M. This feature arises from the virtual lack of dispersion out of the plane of the t_{2g} d orbitals. Therefore, $SrRuO_3$ may be considered to be composed of a set of intersecting planes where the dispersion between adjacent planes and between intersecting planes is minimal.

The effective tight-binding Hamiltonian for the band of predominantly d_{xy} character is given by

$$H_{xy} = \begin{pmatrix} t_{2g} + V_{dd\pi}(\cos q_x + \cos q_y) & 2iV_{pd\pi}\sin\frac{q_x}{2} & 2iV_{pd\pi}\sin\frac{q_y}{2} \\ -2iV_{pd\pi}\sin\frac{q_x}{2} & p_\pi + 2V^{(2)}_{pp\sigma}\cos q_y & 2(V_{pp\sigma} - V_{pp\pi})\sin\frac{q_x}{2}\sin\frac{q_y}{2} \\ -2iV_{pd\pi}\sin\frac{q_y}{2} & 2(V_{pp\sigma} - V_{pp\pi})\sin\frac{q_x}{2}\sin\frac{q_y}{2} & p_\pi + 2V_{pp\sigma}\cos q_x \end{pmatrix}, \quad (1)$$

 ©2004 The American Physical Society

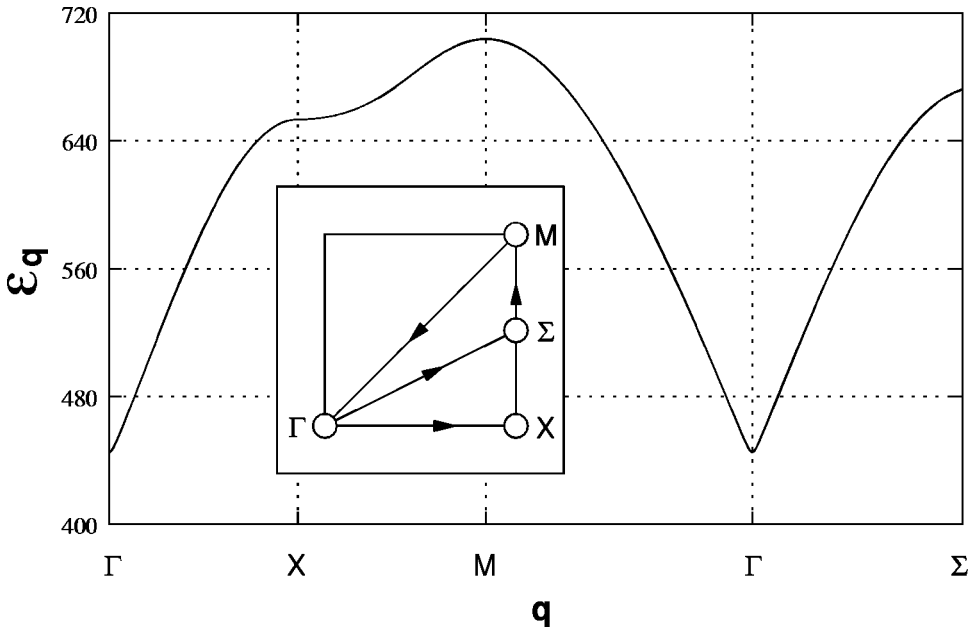

FIG. 1. Effective two-dimensional band structure for hybridized t_{2g}-p_π bands. The energies are given in meV and the inset shows the path connecting the symmetry points in the Brillouin zone.

where the state vector is ordered as d_{xy}, p_y in the $\hat{x}$ direction, and p_x in the $\hat{y}$ direction. The remaining two t_{2g}-p_π bands are obtained by cyclic permutation of the indices. In writing down this Hamiltonian we are ignoring the dispersion out of the plane as well as the coupling between the different t_{2g} bands. The latter effect will be reintroduced as a perturbation in Sec. III and both effects are, in any case, small.

The dispersion relation obtained from Eq. (1) is shown in Fig. 1. The reader is referred to the work of Mazin[12] for the Slater-Koster parameters used in this calculation. It is clear from Fig. 1 that the actual band structure of the system deviates significantly from a model which incorporates only nearest-neighbor hopping. The van-Hove singularity mentioned earlier is not visible in Fig. 1 because only the in-plane momentum vectors are shown. In the out-of-plane direction the bands appear nearly flat as seen in the work of Mazin.[12] In the following section we explore how this additional structure alters the susceptibility of the system to form states with orbital antiferromagnetic and spin antiferromagnetic order.

II. ORBITAL ANTIFERROMAGNETIC SUSCEPTIBILITY

In this section we examine how the susceptibility of the state to OAF order is affected by the band structure discussed in Sec. I. Given the proximity of $SrRuO_3$ to a Mott transition and the large value of the Coulomb repulsion, we believe that a consideration of a generalized t-J model can give insight into the physics of $SrRuO_3$. As the t-J model is the infinite-U limit of the Hubbard model, whether or not this is a good approximation depends on whether $t/U \ll 1$ or, as was suggested by Reischl *et al.*,[13] whether $W/U \leqslant 1$. As mentioned in the Introduction, the value of U is somewhere between 3 and 5 eV. The value of t can be estimated from the band-structure calculations of Mazin[12] and in terms of the Slater-Koster parameters is given by $V_{pd}^2/(\epsilon_d - \epsilon_p)$, which is approximately 1 eV. This gives a value of $t/U \approx 0.25$, suggesting that the t-J model is reasonable in this case. As far as meeting the second phrasing of the criterion is concerned, the analysis is slightly less clear since the work of Reischl *et al.*[13] was conducted for a model with nearest-neighbor hopping where $W = 8t$. This would give a value of $8t/U \approx 2$ for this system, yet the band structure of $SrRuO_3$ is not of this type and the bands are much narrower than the unfrustrated value of $8t$. Therefore, while the use of the t-J model for $SrRuO_3$ certainly pushes the validity of the infinite U limit of the Hubbard model, it gives information about the OAF order in the system that cannot be obtained from a mean-field treatment of the Hubbard model.

Still assuming that the bands are uncoupled, we take as our model the two-dimensional single-band Hamiltonian

$$H = \sum_{\mathbf{q}\sigma} \epsilon_{\mathbf{q}} c^\dagger_{\mathbf{q}\sigma} c_{\mathbf{q}\sigma} + J \sum_{\langle ij \rangle} \boldsymbol{S}_i \cdot \boldsymbol{S}_j , \tag{2}$$

where $\epsilon_{\mathbf{q}}$ is the dispersion relation determined by diagonalizing the Hamiltonian in Eq. (1). In order to obtain the susceptibility we define a set of magnetic quasiparticles via the canonical transformation

$$\begin{pmatrix} \alpha^\dagger_{\mathbf{k}\sigma} \\ \beta^\dagger_{\mathbf{k}\sigma} \end{pmatrix} = \begin{pmatrix} \cos\theta_{\mathbf{k}} & i \sin\theta_{\mathbf{k}} \\ i \sin\theta_{\mathbf{k}} & \cos\theta_{\mathbf{k}} \end{pmatrix} \begin{pmatrix} c^\dagger_{\mathbf{k}\sigma} \\ c_{\mathbf{k}+\mathbf{Q}\sigma} \end{pmatrix}, \tag{3}$$

where the magnetic ordering vector $\mathbf{Q} = \boldsymbol{\pi}$ and lies in the plane of the t_{2g} orbitals. In order to simplify the notation, we assume throughout this section that we are concerned with the d_{xy} orbital.

The onset of orbital antiferromagnetism is characterized by the imaginary part of $\chi_{ij} = \langle c^\dagger_{i\sigma} c_{j\sigma} \rangle$ acquiring a nonzero expectation value. This, in turn, means that there are real microscopic currents circulating around the plaquettes in the lattice. In terms of the quasiparticles in Eq. 3, the orbital order parameter is given by

$$\chi_{ij}=\frac{1}{\mathcal{N}}\sum_{\mathbf{k}}{}' e^{i\mathbf{k}\cdot\mathbf{x}}[\cos(2\theta_{\mathbf{k}})-ie^{i\mathbf{Q}\cdot\mathbf{r}_i}\sin(2\theta_{\mathbf{k}})]\overline{n}_{\mathbf{k}\sigma}, \quad (4)$$

where $\mathbf{x}=\mathbf{r}_i-\mathbf{r}_j$, the prime on the sum indicates that it is restricted to the reduced Brillouin zone, and $\mathcal{N}$ is the number of sites in the lattice. The number operator $\overline{n}$ is the difference in occupancies of the upper and lower magnetic bands: $\overline{n}_{\mathbf{k}\sigma}=\langle\alpha^{\dagger}_{\mathbf{k}\sigma}\alpha_{\mathbf{k}\sigma}-\beta^{\dagger}_{\mathbf{k}\sigma}\beta_{\mathbf{k}\sigma}\rangle$.

Taking the expectation value of the Hamiltonian we obtain

$$\langle H\rangle=\sum_{\mathbf{k}\pm\sigma}E_{\mathbf{k}\pm}n_{\mathbf{k}\pm\sigma}+\frac{3\mathcal{N}J}{4}|\chi|^2, \quad (5)$$

where the number operators $n_{\mathbf{k}\pm\sigma}$ correspond to the upper $(+)$ and lower $(-)$ magnetic bands. Implicit in Eq. (5) is the fact that we are dealing with Fock states so that the biquadratic term in the Hamiltonian factorizes. $E_{\mathbf{k}\pm}$ defines the magnetic band energies:

$$E_{\mathbf{k}\pm}=\frac{\epsilon_{\mathbf{k}}+\epsilon_{\mathbf{k}+\mathbf{Q}}}{2}\pm\left[\left(\frac{\epsilon_{\mathbf{k}}-\epsilon_{\mathbf{k}+\mathbf{Q}}}{2}-\frac{3J}{4}\times\mathrm{Re}[\chi](\cos k_x+\cos k_y)\right)\cos(2\theta_{\mathbf{k}})+\frac{3J}{4}\mathrm{Im}[\chi](\cos k_x-\cos k_y)\sin(2\theta_{\mathbf{k}})\right]. \quad (6)$$

Since minimizing Eq. (5) with respect to $\mathrm{Re}[\chi]$ and $\mathrm{Im}[\chi]$ reproduces Eq. (4), we can treat these as variational parameters independent of the $\theta_{\mathbf{k}}$. Eq. (5) can then be minimized in order to determine the angles $\theta_{\mathbf{k}}$ and upon substitution yields

$$E_{\mathbf{k}\pm}=\frac{\epsilon_{\mathbf{k}}+\epsilon_{\mathbf{k}+\mathbf{Q}}}{2}\pm\left[\left(\frac{\epsilon_{\mathbf{k}}-\epsilon_{\mathbf{k}+\mathbf{Q}}}{2}-\frac{3J}{4}\times\mathrm{Re}[\chi](\cos k_x+\cos k_y)\right)^2+\left(\frac{3J}{4}\mathrm{Im}[\chi](\cos k_x-\cos k_y)\right)^2\right]^{1/2}. \quad (7)$$

The mean-field equations are then obtained by minimizing with respect to the order parameters. Defining $E_0=\Sigma_{\mathbf{k}\pm\sigma}E_{\mathbf{k}\pm}n_{\mathbf{k}\pm\sigma}$ the equations read

$$\frac{\partial E_0}{\partial\mathrm{Re}[\chi]}+\frac{3\mathcal{N}J}{2}\mathrm{Re}[\chi]=0, \quad (8)$$

$$\frac{\partial E_0}{\partial\mathrm{Im}[\chi]}+\frac{3\mathcal{N}J}{2}\mathrm{Im}[\chi]=0. \quad (9)$$

The susceptibility to form an OAF state follows from the second of these equations. We can rewrite this in terms of a Stoner criterion $J\chi_{OAF}=1$ where

$$\chi_{OAF}=\frac{3}{2\mathcal{N}}\sum_{\mathbf{k}}{}'\frac{(\cos k_x-\cos k_y)^2(n_{\mathbf{k}}-n_{\mathbf{k}+\mathbf{Q}})}{\epsilon_{\mathbf{k}}-\epsilon_{\mathbf{k}+\mathbf{Q}}-3J\mathrm{Re}[\chi](\cos k_x+\cos k_y)/2}. \quad (10)$$

This should be compared with the susceptibility for a spin antiferromagnetic state which is almost identical except for the factor in the numerator:

$$\chi_{SAF}=\frac{4}{\mathcal{N}}\sum_{\mathbf{k}}{}'\frac{(n_{\mathbf{k}}-n_{\mathbf{k}+\mathbf{Q}})}{\epsilon_{\mathbf{k}}-\epsilon_{\mathbf{k}+\mathbf{Q}}-3J\mathrm{Re}[\chi](\cos k_x+\cos k_y)/2}. \quad (11)$$

Note that Eqs. (10) and (11) are completely general for models of the form in Eq. (2). Here, we are interested in the effect of the $\epsilon_{\mathbf{q}}$ term on these susceptibilities. While the propensity to order for both types of magnetic systems relies on the nesting of the Fermi surface at the ordering wave vector $\mathbf{Q}$, this nesting is only important around the points X in the OAF system (see Fig. 1) due to the vanishing of the numerator around the points $k_x=k_y$.

Numerical calculation of the susceptibility for the orbital antiferromagnetic state is not entirely trivial, as one must solve the simultaneous integral Eqs. (8) and (10). In addition, the occupancies $n_{\mathbf{k}}$ appearing in these equations are determined by δ and the magnetic band energies in Eq. (7). Since we are looking for the critical value of J at which the system acquires a nonzero value of $\mathrm{Im}[\chi]$, we can set this equal to zero in Eqs. (7) and (8). The occupancies are then entirely determined by the product $J\mathrm{Re}[\chi]$. This in turn determines $\mathrm{Re}[\chi]$ (and hence J) through Eq. (8), which can be written out explicitly as

$$\mathrm{Re}[\chi]=\frac{1}{\mathcal{N}}\sum_{\mathbf{k}}{}'(\cos k_x+\cos k_y)(n_{\mathbf{k}}-n_{\mathbf{k}+\mathbf{Q}}). \quad (12)$$

In this way $\mathrm{Re}[\chi]$ is determined as a function of J. The solution of the Stoner criterion using Eq. (10) is then a single integral equation for J, whose solution is straightforward.

Figure 2 shows the values of J for which the Stoner criterion is satisfied for the susceptibilities in Eqs. (10) (solid line) and (11) (dashed line) for a range of doping $\delta=1-\mathcal{N}_e/\mathcal{N}$. The spin-exchange energy has been scaled to the bandwidth $W=259$ meV. It is noteworthy that around the point $\delta=-1/4$ the orbital antiferromagnetic state forms at a lower value of J than the spin antiferromagnetic state. This behavior is entirely due to incorporating the realistic band structure discussed in Sec. I into the model. In models with only near-neighbor hopping, the analogous calculation shows that the susceptibility is always larger for the SAF than the OAF state. Two points should be noted in regards to Fig. 2. The first is that away from $\delta=0$ there are terms which should strictly be included in the Hamiltonian of order t/U, but that have been neglected in adopting the t-J model in Eq. (2). Second, while the trends seen here undoubtedly persist, it is not clear to what degree the numerical values for J, and indeed the presence or absence of a crossing in the susceptibilities, would be altered if one went beyond the mean-field treatments employed in this paper.

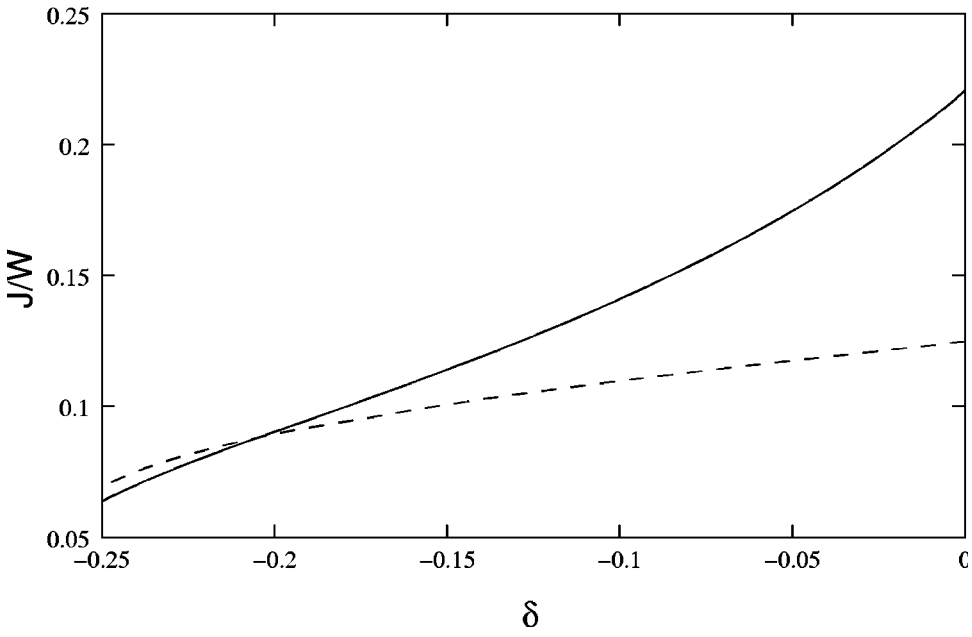

FIG. 2. Susceptibility to OAF (solid line) and SAF (dashed line) as a function of doping δ and the ratio of the spin exchange to the bandwidth: J/W. Not shown in the figure is that below $\delta \approx -1/4$ the critical value of J rises rapidly for both types of order.

We have also calculated the magnetization of the model by solving Eqs. (8) and (9) numerically using 10^6 momentum points. Figure 3 shows the flux per plaquette determined from

$$\Phi = \sum_{\text{plaquette}} \arctan \frac{\text{Im}[\chi]}{\text{Re}[\chi]}. \tag{13}$$

The different curves are for different values of J/W ranging from 0.1 to 0.3. While the susceptibility reaches its largest value around $\delta = -1/4$, the magnetization is largest near $\delta = 0$. In the following section we will perform all calculations for $J = 0.3W$ and at half filling where the flux order is well developed: $\Phi = 2/3$.

III. COUPLING

In order to take into account the effect of interplane coupling on the system we add a term to the Hamiltonian in Eq. (2) of the form

$$H' = \sum_{ij} \sum_{\sigma} \sum_{\nu \neq \nu'} t_{ij}^{\nu\nu'} c_{i\nu\sigma}^{\dagger} c_{j\nu'\sigma}, \tag{14}$$

which will be treated as a perturbation. The first nonvanishing correction to the energy will be second order in $t^{\nu\nu'}$. This perturbation may be rewritten in momentum space as

$$H' = \sum_{\mathbf{q}\sigma} \sum_{\nu \neq \nu'} T_{\nu\nu'}(\mathbf{q}) c_{\mathbf{q}\nu\sigma}^{\dagger} c_{\mathbf{q}\nu'\sigma}, \tag{15}$$

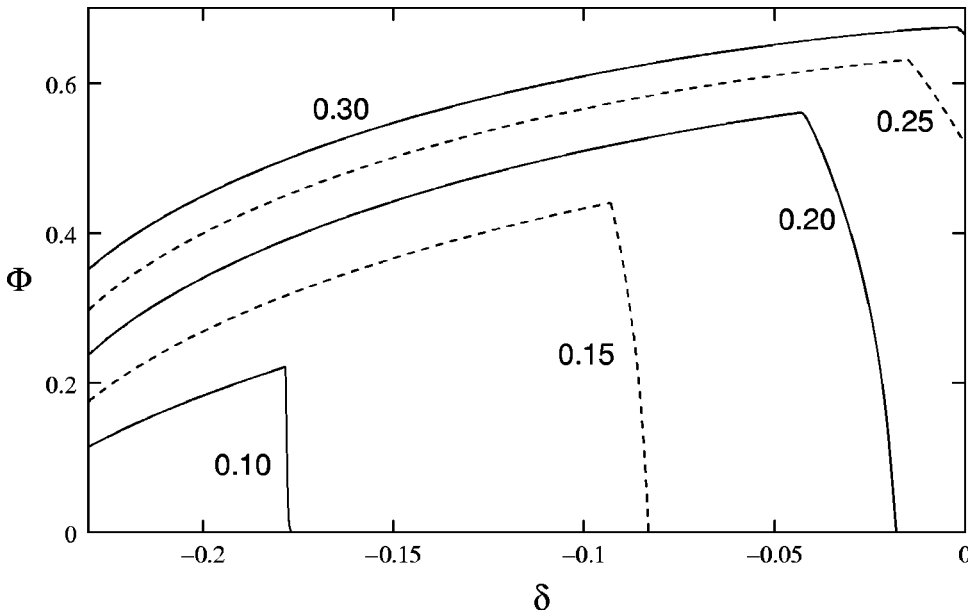

FIG. 3. Flux per plaquette Φ as a function of doping δ. The different curves are for different values of J/W.

TABLE I. Momentum ordering vectors for coupled plane model.

$\mathbf{Q}_1$	$\mathbf{Q}_2$	$\mathbf{Q}_3$	$\mathbf{Q}_4$	$\mathbf{Q}_5$	$\mathbf{Q}_6$	$\mathbf{Q}_7$	$\mathbf{Q}_8$
0	$\pi\hat{\boldsymbol{x}}$	$\pi\hat{\boldsymbol{y}}$	$\pi\hat{\boldsymbol{z}}$	$\pi(\hat{\boldsymbol{x}}+\hat{\boldsymbol{y}})$	$\pi(\hat{\boldsymbol{y}}+\hat{\boldsymbol{z}})$	$\pi(\hat{\boldsymbol{z}}+\hat{\boldsymbol{x}})$	$\boldsymbol{\pi}$

where we have defined:

$$T_{\nu\nu'}(\mathbf{q})=\sum_j e^{i\mathbf{q}\cdot(\mathbf{r}_i-\mathbf{r}_j)}t_{ij}^{\nu\nu'}. \tag{16}$$

Note that due to translational invariance there is no dependence of $T_{\nu\nu'}$ on i. Based on the form of the tight-binding Hamiltonian[12] we take this to be

$$T_{xy,yz}=t'\sin q_x \sin q_z, \tag{17}$$

and cyclic permutations thereof. The end results of the calculation will turn out to be rather insensitive to the actual form of the hopping matrix element.

For each band there is a doubling of the unit cell with the onset of orbital order. However, the ordering wave vectors are not the same in the three bands and this requires rewriting the Hamiltonian in terms of an eight-atom unit cell. We therefore take

$$H'=\sum_{\mathbf{q}}{}' \sum_{\nu\neq\nu'} \sum_{\sigma} \sum_{i=1}^{8} T_{\nu\nu'}(\mathbf{q}+\mathbf{Q}_i)c^{\dagger}_{\mathbf{q}+\mathbf{Q}_i\nu\sigma}c_{\mathbf{q}+\mathbf{Q}_i\nu'\sigma}, \tag{18}$$

where the prime on the momentum sum indicates that we only sum over the reduced cubic Brillouin zone and where the ordering vectors $\mathbf{Q}_i$ are given in Table I.

For a given band ν, the orbital order is given by

$$\chi_{ij}^{\nu}=\mathrm{Re}[\chi]+ie^{ic_\nu\pi}e^{i\mathbf{Q}_\nu\cdot\mathbf{r}_i}e^{i\pi(x_j^{\nu_2}-x_i^{\nu_2})}\mathrm{Im}[\chi], \tag{19}$$

where ν_2 is the Cartesian index corresponding to the second in-plane direction of the given band (i.e., y for the xy band), $\mathbf{Q}_\nu$ is the ordering vector for that band, and $c_\nu=0,1$ shifts the current pattern by one lattice site. This last term is important since it affects the overlap of intersecting planes. For each band, the ordering wave vector has two possible values, corresponding to currents which align or antialign in adjacent planes. These can be summarized as

$$\mathbf{Q}_\nu=\pi(\hat{\boldsymbol{x}}_{\nu_1}+\hat{\boldsymbol{x}}_{\nu_2}+p_\nu\hat{\boldsymbol{x}}_{\nu_3}), \tag{20}$$

where $p_\nu=0$ (aligned) or 1 (antialigned) and where ν_3 is the out-of-plane Cartesian index (i.e., z for the xy band). In the absence of coupling, there is no difference in the energies of the states for different values of the c_ν and p_ν. After adding the perturbation, we will calculate the response of the system to the perturbation for all 2^6 configurations arising from p_ν, $c_\nu=\{0,1\}$.

The effects of the c_ν are shown in Fig. 4. In Fig. 4(a), corresponding to $c_\nu=0$ for all ν, the currents cancel along the three bonds intersecting the origin. The remainder of the currents in the lattice are only determined when the p_ν have been specified, determining whether the currents in adjacent planes are aligned or antialigned. Figure 4(b) shows the effect of switching one of the c_ν's, causing the currents to add along two of the three bands intersecting the origin. It should be clear from the figure that there is no configuration where the currents add along all of the bonds.

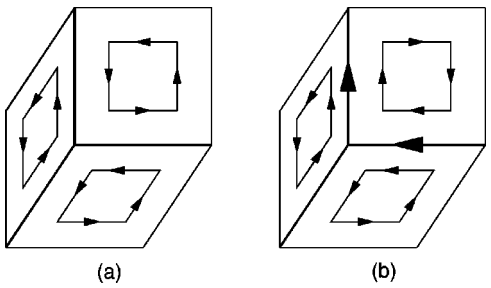

FIG. 4. Current distributions for intersecting plane model. The insets in each of the plaquettes show the direction of the currents in that planar band. The dark lines show the net current flowing along the bonds. Two configurations are shown: (a) in which the currents cancel along the three dark bonds intersecting the origin and (b) in which they add along two of the three bonds.

Given the orbital order in Eq. (19), and dropping the irrelevant spin index, the Hamiltonian for the system may be written as

$$H_\nu=\frac{3\mathcal{N}J}{4}+\sum_{\mathbf{q}} \psi^{\dagger}_{\nu\mathbf{q}}h_\nu(\mathbf{q})\psi_{\nu\mathbf{q}}, \tag{21}$$

where $\psi^{\dagger}_{\mathbf{q}}=(c^{\dagger}_{\mathbf{q}+\mathbf{Q}_1},\ldots,c^{\dagger}_{\mathbf{q}+\mathbf{Q}_8})$. The matrix $h_\nu(\mathbf{q})$ is given by

$$\begin{aligned}[h_\nu(\mathbf{q})]_{ij}=&\left\{\epsilon_{\mathbf{q}+\mathbf{Q}_i}+\frac{3J}{4}\mathrm{Re}[\chi]\sum_{k=1}^{2}\cos(\mathbf{q}+\mathbf{Q}_i)_{\nu_k}\right\}\delta_{ij}\\ &-\frac{3iJ}{4}e^{i\pi c_\nu}\mathrm{Im}[\chi]\sum_{k=1}^{2}(-1)^k\cos(\mathbf{q}+\mathbf{Q}_i)_{\nu_k}\\ &\times\delta(\mathbf{Q}_i-\mathbf{Q}_j-\mathbf{Q}_\nu).\end{aligned} \tag{22}$$

This Hamiltonian is solved numerically to obtain the eight magnetic quasiparticles for each of the three bands ν. Upon inversion, the solution is of the form

$$c^{\dagger}_{\mathbf{q}+\mathbf{Q}_i\nu\sigma}=\sum_{z=1}^{4}[a(\mathbf{q},\nu,i,z)\alpha^{\dagger}_{z\mathbf{q}\nu\sigma}+b(\mathbf{q},\nu,iz)\beta^{\dagger}_{z\mathbf{q}\nu\sigma}], \tag{23}$$

where the label z indexes the magnetic bands and the α and β particles correspond to the upper and lower magnetic bands, respectively, as they did in Eq. (3).

We assume that the term t' appearing in Eq. (14) is small so that we can consider only the first nonvanishing term in the perturbation. For simplicity, we also assume that the system is at half filling. This means that we can ignore all terms in the perturbing Hamiltonian which contain α, since all the states in the lower magnetic bands will be filled. The perturbation is then given by

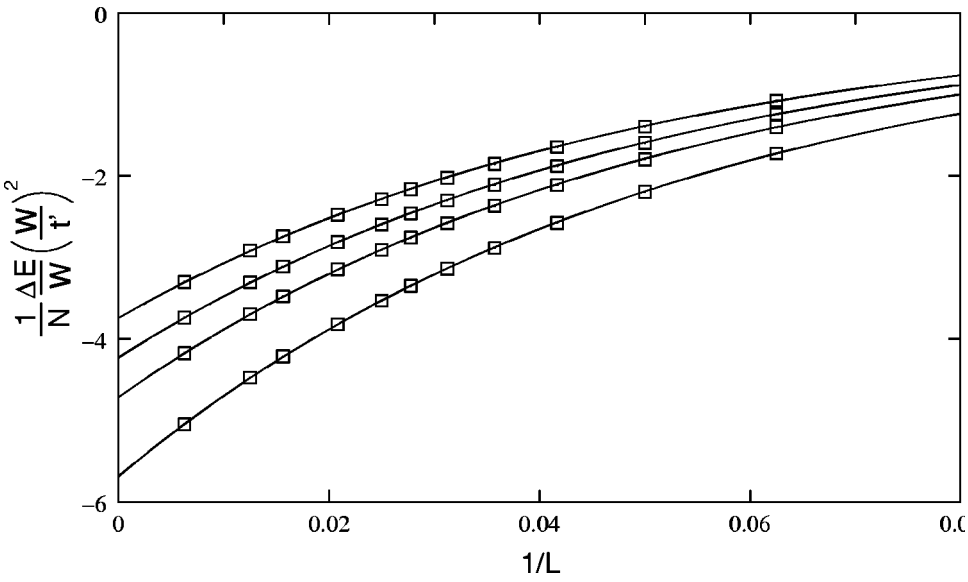

FIG. 5. The energy-level splittings as a function of $1/L$ for which the calculation was performed. The curves show the extrapolations to $L=\infty$.

$$H' \doteq \sum_{\mathbf{q}}{}' \sum_{\nu\neq\nu'} \sum_{\sigma} \sum_{z,z'=1}^{4} \tau^{zz'}_{\nu\nu'}(\mathbf{q})\alpha^{\dagger}_{z\mathbf{q}\nu\sigma}\beta_{z'\mathbf{q}\nu'\sigma}, \quad (24)$$

where the dot signifies that the equality is only strictly true when the perturbing Hamiltonian acts to the left on the ground state at half filling. The effective hopping parameter between the magnetic bands is given by

$$\tau^{zz'}_{\nu\nu'}(\mathbf{q}) = \sum_{i=1}^{8} T_{\nu\nu'}(\mathbf{q}+\mathbf{Q}_i)a(\mathbf{q},\nu,i,z)b^{*}(\mathbf{q},\nu' i,z'). \quad (25)$$

The excited states of interest are those with a single particle-hole pair created out of the ground state. These are of the form: $|\Psi_X\rangle = \beta^{\dagger}_{y\mathbf{k}\mu\eta}\alpha_{y'\mathbf{k}\mu'\eta'}|\Psi_0\rangle$, where $|\Psi_0\rangle$ is the Fock state with the lower magnetic bands filled. Including contributions to second order in t', the energy shift of the ground state will be given by

$$\Delta E = \sum_{X} \frac{|\langle\Psi_0|H'|\Psi_X\rangle|^2}{E_0 - E_X} \quad (26)$$

$$= 2\sum_{\mathbf{q}}{}' \sum_{\nu\neq\nu'} \sum_{z,z'=1}^{4} \frac{|\tau^{zz'}_{\nu\nu'}(\mathbf{q})|^2}{\epsilon^{-}_{z'\nu'\mathbf{q}} - \epsilon^{+}_{z\nu\mathbf{q}}}, \quad (27)$$

where $\epsilon^{\pm}$ refer to the energies of the quasiparticles in the upper and lower magnetic bands and where the factor of 2 comes from the sum over spin.

Equation (27) has been solved numerically to obtain the energy splittings; the results are shown in Fig. 5. The calculations were performed at the point $J=0.3W$ and $\delta=0$, corresponding to a magnetization of $\Phi=2/3$. The calculation is performed using $\mathcal{N}=L^3$ momentum points, diagonalizing the Hamiltonian in Eq. (22) at each momentum point to find the eigenstates and eigenvalues, and using these to compute the

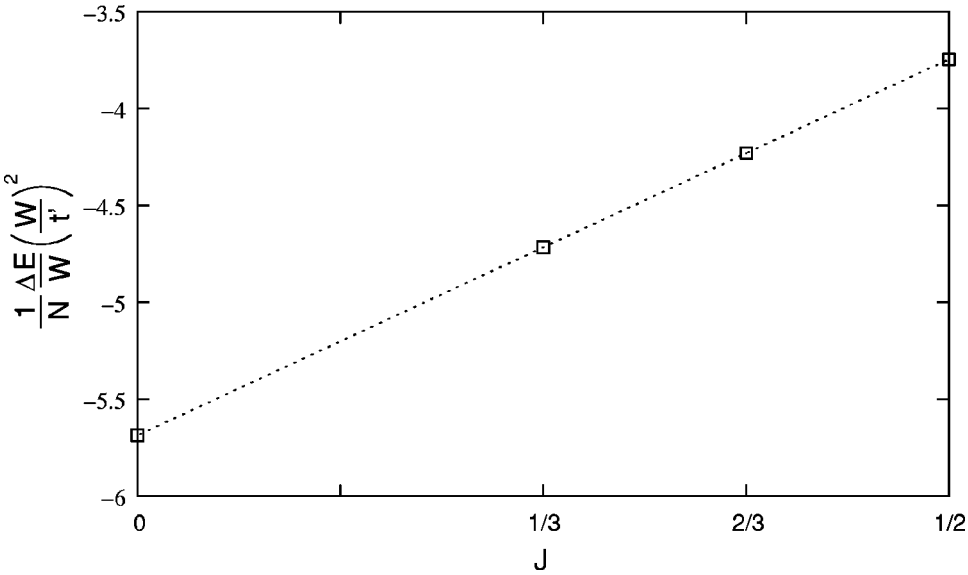

FIG. 6. Energy-level splittings as a function of the number of bonds carrying current in the eight-atom unit cell. The four data points correspond to the only four possibilities for net current: current on 0, 1/3, 1/2, or 2/3 of all bonds. The dotted line is a linear fit through the four data points.

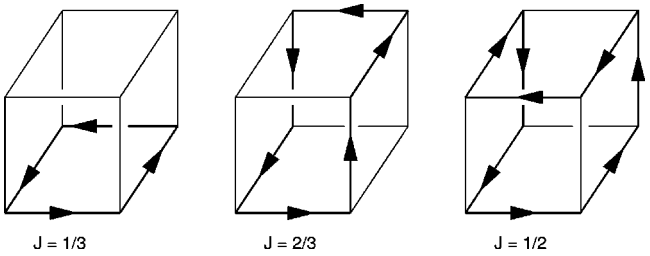

FIG. 7. Current distributions for representative states with $J=1/3$, 1/2, and 2/3. The $J=0$ state is not shown.

terms in Eqs. (25) and (27). The calculation is performed for all possible combinations of the c_ν and p_ν for a range of L values as shown in Fig. 5.

In the presence of the perturbation, the degenerate states are split into four distinct states. These can be uniquely labeled by the number of bonds which carry current within the eight–atom unit cell. As the readers may convince themselves by drawing cubes ad nausea, there are only four distinct states. Either all of the currents cancel out between the intersecting planes, or currents remain on 1/3 of the bonds, on 1/2 of the bonds, or on 2/3 of the bonds. This is a purely geometrical constraint owing to the fact that all current loops must close on themselves. Representative states for each of the current-carrying configurations are shown in Fig. 7.

The data from Fig. 5 are used to extrapolate to $L=\infty$ using an exponential fit: $f(L)=a\exp[-b/L]$; the results of this are shown in Fig. 6. The calculation was performed for all 2^6 possible choices of the c_ν, p_ν, and all of these fall directly onto one of the four data points shown in the figure. The calculation clearly demonstrates that the coupling to the perturbation depends only on the total current in the unit cell and is linear in this quantity, a fact which is not obvious from the form of Eq. (27). The state which couples most strongly to the perturbation is the state where all the currents cancel, which requires $p_\nu=1$ for all ν and that the c_ν be equal.

IV. DISCUSSION

We propose that the pseudogap state seen in the cubic transition metal oxides may be described by a set of intersecting planes in which orbital antiferromagnetic order has developed. The deviation of the tight-binding model from nearest-neighbor hopping leads to regions of δ where the susceptibility to orbital antiferromagnetism, or flux order, is actually larger than the susceptibility to spin antiferromagnetism, or Néel order. As this result is based on a mean-field treatment, future work will be done to numerically verify whether or not this effect persists when the constraint on double occupancy is strictly enforced. In these coupled planar systems, coupling between the bands selects a configuration in which the currents along all bonds cancel perfectly. Since there are no net currents on the bonds, experiments such as neutron diffraction which have been proposed to determine the presence of orbital order in two[14] and three[1] dimensions will not be effective probes for this system. Even though the net current in the sample is predicted to be zero, the electrons are in a true orbital antiferromagnetic state, and signatures from optical conductivity measurements[1] will still be present. Future work should center around how to measure OAF order without directly measuring the local magnetic fields in the sample.

ACKNOWLEDGMENTS

We would like to thank J. Franklin for many useful discussions. We acknowledge support from the DOE through the Complex Materials Program at SSRL.

*Electronic address: Darrell.Schroeter@Directory.Reed.EDU

[1] D.F. Schroeter and S. Doniach, Phys. Rev. B **66**, 75 120 (2002).
[2] D.F. Schroeter, Ph.D. thesis, Stanford University, 2002.
[3] P. Kostic, Y. Okada, N.C. Collins, Z. Schlesinger, J.W. Reiner, L. Klein, A. Kapitulnik, T.H. Geballe, and M.R. Beasley, Phys. Rev. Lett. **81**, 2498 (1998).
[4] I. Affleck and J.B. Marston, Phys. Rev. B **37**, 3774 (1988).
[5] J.S. Ahn, J. Bak, H.S. Choi, T.W. Noh, J.E. Han, Y. Bang, J.H. Cho, and Q.X. Jia, Phys. Rev. Lett. **82**, 5321 (1999).
[6] K. Fujioka, J. Okamoto, T. Mizokawa, A. Fujimori, I. Hase, M. Abbate, H.J. Lin, C.T. Chen, Y. Takeda, and M. Takano, Phys. Rev. B **56**, 6380 (1997).
[7] L. Klein, J.S. Dodge, C.H. Ahn, J.W. Reiner, L. Mieville, T.H. Geballe, M.R. Beasley, and A. Kapitulnik, J. Phys.: Condens. Matter **8**, 10 111 (1996).
[8] V.J. Emery and S.A. Kivelson, Phys. Rev. Lett. **74**, 3253 (1995).
[9] M.S. Laad and E. Müller-Hartmann, Phys. Rev. Lett. **87**, 246402 (2001).
[10] A. Liebsch, Eur. Phys. J. B **32**, 477 (2003).
[11] B.C. Chakoumakos, S.E. Nagler, S.T. Misture, and H.M. Christen, Physica B **241–243**, 358 (1997).
[12] I.I. Mazin, D.A. Papaconstantopoulos, and D.J. Singh, Phys. Rev. B **61**, 5223 (2000).
[13] A. Reischl, E. Müller-Hartmann, and G.S. Uhrig, cond-mat/0401028 (unpublished).
[14] T.C. Hsu, J.B. Marston, and I. Affleck, Phys. Rev. B **43**, 2866 (1991).